

1 **Effect of water vapour on the determination of Aerosol Direct Radiative Effect based on the**  
2 **AERONET fluxes**

3 **J. Huttunen<sup>1,2</sup>, A. Arola<sup>1</sup>, G. Myhre<sup>3</sup>, A.V. Lindfors<sup>1</sup>, T. Mielonen<sup>1</sup>, S. Mikkonen<sup>2</sup>, J. S. Schafer<sup>4</sup>, S.**  
4 **N. Tripathi<sup>5</sup>, M. Wild<sup>6</sup>, M. Komppula<sup>1</sup> and K. E. J. Lehtinen<sup>1,2</sup>**

5 [1]{Finnish Meteorological Institute (FMI), Kuopio Unit, Finland.}

6 [2]{Department of Applied Physics, University of Eastern Finland, Kuopio, Finland.}

7 [3]{Center for International Climate and Environmental Research - Oslo, Norway.}

8 [4]{NASA/Goddard Space Flight Center (GSFC), Biospheric Sciences Branch, Greenbelt, MD, USA.}

9 [5]{Department of Civil Engineering, Indian Institute of Technology, Kanpur, India.}

10 [6]{Institute for Atmospheric and Climate Science, ETH Zurich, Switzerland.}

11 Corresponding author: J. Huttunen, Finnish Meteorological Institute, Kuopio Unit, P.O. Box  
12 1627, FI-70211 Kuopio, Finland. (jani.huttunen@fmi.fi)

13

14 **Abstract**

15 The Aerosol Direct Radiative Effect (ADRE) is defined as the change in the solar radiation flux,  $F$ , due  
16 to aerosol scattering and absorption. The difficulty in determining ADRE stems mainly from the need  
17 to estimate  $F$  without aerosols,  $F^0$ , with either radiative transfer modelling and knowledge of the  
18 atmospheric state, or regression analysis of radiation data down to zero aerosol optical depth (AOD), if  
19 only  $F$  and AOD are observed. This paper examines the regression analysis method by using modeled  
20 surface data products provided by the AEROSOL ROBOTIC NETWORK (AERONET). We extrapolated  $F^0$  by  
21 two functions: a straight linear line and an exponential nonlinear decay. The exponential decay  
22 regression is expected to give a better estimation of ADRE with a few percents larger extrapolated  $F^0$   
23 than the linear regression. We found that, contrary to the expectation, in most cases the linear

24 regression gives better results than the nonlinear. In such cases the extrapolated  $F^0$  represents an  
25 unrealistically low water vapour column (WVC), resulting in underestimation of attenuation caused by  
26 the water vapour, and hence too large  $F^0$  and overestimation of the magnitude of ADRE. The nonlinear  
27 ADRE is generally 40-50 % larger in magnitude than the linear ADRE due to the extrapolated  $F^0$   
28 difference. Since for a majority of locations, AOD and WVC have a positive correlation, the  
29 extrapolated  $F^0$  with the nonlinear regression fit represents an unrealistically low WVC, and hence too  
30 large  $F^0$ . The systematic underestimation of  $F^0$  with the linear regression is compensated by the positive  
31 correlation between AOD and water vapour, providing the better result.

32

### 33 **1. Introduction**

34 Significant uncertainties exist in the current estimates of aerosol effects on climate (IPCC, 2013). This  
35 holds also for the aerosol direct radiative effect (ADRE) and aerosol direct radiative forcing (ADRF).  
36 The ADRE defines the attenuation of the (cloud free sky) surface solar radiation flux ( $F$ ) due to aerosol  
37 scattering and absorption. Herein, we consider the solar radiation flux at the surface, although ADRE  
38 applies also for the longwave flux and above the atmosphere. In the definitions of ADRE and ADRF,  
39 effects relate to both anthropogenic and natural aerosol particles, while forcing refers to the impact of  
40 anthropogenic aerosol particles. Although, e.g., Myhre (2009) recently showed an increment of the  
41 consistency between observation based and global aerosol model estimates, with a reduction in the  
42 uncertainty of this effect, other studies (e.g., Loeb and Su, 2010) highlight that considerable  
43 uncertainties are still associated with ADRE, mainly due to the uncertainties in single scattering albedo  
44 (SSA). Satheesh and Ramanathan (2000) employed a method in which ADRE is estimated using the  
45 aerosol direct effect efficiency (ADREE), which is the ADRE normalized by the aerosol optical depth  
46 (AOD), and it is estimated by fitting a straight line into surface solar flux and AOD observations. A

47 linear dependence between aerosol attenuation and AOD has been commonly assumed when estimating  
48 ADRE (e.g., Kaufman et al., 2002; Bush and Valero, 2002, 2003; Dumka et al., 2006; Roger et al.,  
49 2006; di Sarra et al., 2008; Garcia et al., 2009; Satheesh et al., 2010). Typical attenuation of radiation  
50 intensity, however, implies nonlinear decay, as considered by e.g. Conant et al. (2003), Markowicz et  
51 al. (2008) and Kudo et al. (2010). Thus, a linear fit to  $F$  and AOD data may result in an incorrect  
52 extrapolation of  $F_0$ .

53 The aim of this paper is to examine the uncertainties involved in estimating ADRE, both using  
54 the linear fitting method and a nonlinear approach if  $F$  and AOD data are available from surface or  
55 satellite measurements. For this, we use Aerosol Robotic Network (AERONET) products  
56 (<http://aeronet.gsfc.nasa.gov/>) from all available AERONET stations, which cover different aerosol  
57 types and surface reflectance properties and provide modelled surface solar radiation fluxes also. We  
58 conducted our analysis using these modeled fluxes since they represent realistically enough the aerosol-  
59 induced relative changes in  $F$  and furthermore give an estimate for  $F^0$ , which is self-consistent within  
60 the selected  $F$  (AOD) data set. As AERONET provides an estimation of  $F^0$ , we can compare the  
61 estimations immediately with the baseline (AERONET). Special attention is paid to the possible effect  
62 of water vapour on estimating ADRE.

63

## 64 **2. Methods and data**

65 AERONET is a ground-based remote-sensing global network of Cimel sun photometers (Holben et al.,  
66 1998) including the AERONET inversion code with radiative transfer code implementation. The  
67 inversion strategy, described in Dubovik and King (2000), provides a group of parameters, e.g. AOD,  
68 Ångström exponent (AE) and water vapour column (WVC) from the sun measurements and e.g. SSA,

69 asymmetry parameter (ASYM) and size distribution from the sky measurements. AOD is provided with  
70 wavelength channels 340, 380, 440, 500, 670, 870, 1020 and 1640 nm (all or some of these, depending  
71 on site of AERONET), WVC from 940 nm and e.g. SSA and ASYM from 440, 670, 870 and 1020 nm.  
72 The Discrete Ordinates (DISORT) provides broadband fluxes (both at the top of atmosphere and at the  
73 surface, with and without aerosols), calculated with the correlated-k distribution in the Global  
74 Atmospheric Model (GAME) code from 200 nm to 4000 nm. The ozone is based on monthly averaged  
75 climatology by the Total Ozone Mapping Spectrometer (TOMS). Moreover, the US standard 1976  
76 atmosphere model sets the atmospheric gaseous profile. The surface reflectivity is approximated by the  
77 Bidirectional Reflectance Distribution Function (BRDF) and observations from the Moderate-  
78 Resolution Imaging Spectroradiometer (MODIS). More details about the AERONET description from  
79 e.g. García et al. (2012). The uncertainty of AOD is 0.01-0.02 depending on the wavelength (Eck et al.,  
80 1999), the uncertainty in SSA is approximately 0.03 (Dubovik et al., 2000), and the uncertainty in  
81 WVC of 12 % (Holben et al., 1998). We used broad-band modeled surface shortwave fluxes from this  
82 data set. In this study, level 1.5 sky AERONET data are divided into groups by station, season  
83 (December-February, March-May, June-August and September-November) and by solar zenith angle  
84 (SZA) ( $3^\circ$  steps in the range  $0^\circ$ - $80^\circ$ ). A dataset was included in the analysis if it had at least 20  
85 observations and the data contained AOD 550 nm values above 0.3 and below 0.1. We chose to use  
86 level 1.5 data because using level 2.0 would leave out all quality-assured data with AOD 440 nm  $< 0.4$   
87 (including e.g. quality assured SSA and  $F$  calculations). The drawback of this choice is that at these low  
88 values of AOD, there are significant uncertainties in the optical properties retrieved. This is especially  
89 true for SSA, which is an important parameter. Thus, we applied all other level 2 criteria except for  
90 AOD (and SZA) limit, in order to enhance the accuracy of the data set selected. Moreover, we have  
91 imposed an additional data flagging criterion, removing those SSA points at the AOD 440 nm  $< 0.4$ ,  
92 which are outside the average SSA  $\pm$  standard deviation, defined for the AOD 440 nm  $> 0.4$ .

93 ADRE at the surface is the difference between the solar flux with and without aerosols: ADRE  
 94  $= \Delta F = F^{aer} - F^0$  ( $F^{aer}$  is flux with aerosols). The major challenge obviously is the determination of  $F^0$ .  
 95 The methodology for its estimation employed in this study is illustrated in Fig. 1, in which  $F^{aer}$   
 96 (+symbols) is plotted as a function of AOD (from now on 550 nm) for the AERONET site in Kanpur  
 97 station (26° N, 80° E) for the spring months March-May with  $SZA = 69^\circ \pm 1.5^\circ$  ( $F^{aer}$  values were  
 98 normalized for the average earth-sun distance and cosine correction of  $F^{aer}$  was done within SZA  
 99 ranges to its midpoints).  $F^0$  represents the case AOD = 0, but with measurements only at AOD above  
 100 ca. 0.15, we have to extrapolate down to 0. In Fig. 1 we show two such extrapolations: a linear fit  
 101 (dashed line) and an nonlinear decay fit (solid line) with the data.

102 We chose this data subset since it represent a case in which the  $F^{aer}$  and AOD data exhibit the  
 103 natural nonlinear behavior of radiation intensity decay. Thus the resulting intercepts of the two curves  
 104 at AOD = 0 are quite different, 317  $Wm^{-2}$  with linear extrapolation and 349  $Wm^{-2}$  with nonlinear  
 105 regression, with a difference of 32  $Wm^{-2}$  when estimating ADRE. Also, for each  $F^{aer}$  we show the  
 106 corresponding AERONET  $F^0$  (circles), based on the retrieved WVC and surface albedo, and calculated  
 107 with a radiative transfer model (e.g., Garcia et al., 2008; Derimian et al., 2008). We use the ADRE  
 108 obtained by averaging these  $F^0$  (circles) values (bar at  $F = 325 Wm^{-2}$  on the y-axis) as the benchmark  
 109 against which the extrapolation methods are evaluated.

110 Mathematically, our analysis can be summed up as a comparison between the extrapolated  
 111 ADRE

$$112 \quad ADRE_{extrapol} = \frac{1}{n} \sum F_i^{aer} - F_{extrapol}^0 \quad (1)$$

113 and the AERONET ADRE

$$114 \quad ADRE_{AERONET} = \frac{1}{n} \sum F_i^{aer} - \frac{1}{n} \sum F_i^0, \quad (2)$$

115 in where  $F_i^{aer}$  and  $F_i^0$  is  $F^{aer}$  and  $F^0$ , respectively, with  $i$  varying from one to the number of dataset,  $n$ .

116 Notably, the extrapolated  $F^0$  ( $F^0_{extrapol}$ ) derived with fits represents a single value for a dataset, but in the  
 117 AERONET,  $F^0$  is determined side-by-side with each  $F^{aer}$ .  $F^0_{extrapol}$  is calculated using fits as follows

$$118 \quad F_i^{nonlin} = x_1 + x_2 * \exp(-x_3 * AOD_i); F_{extrapol}^{0,nonlin} = x_1 + x_2, \quad (3)$$

$$119 \quad F_i^{lin} = x'_1 + x'_2 * AOD_i; F_{extrapol}^{0,lin} = x'_1, \quad (4)$$

120 in where  $F_i^{nonlin}$  and  $F_i^{lin}$  is estimated  $F^{aer}$  derived for each AOD with the nonlinear and linear method,  
 121 respectively. Constants of fits are  $x_1, x_2, x_3, x'_1$  and  $x'_2$ , and  $F_i^{0,nonlin}$  and  $F_i^{0,lin}$ , thus  $F^0_{extrapol}$  of the nonlinear  
 122 and linear fits, are provided with the constants.

123 Our decision to use the modeled  $F$  from AERONET, instead of pyranometer measurements, was  
 124 based on two different aspects. First, this allowed us to include a multiple number of sites, with very  
 125 different and varying aerosol conditions. Second, AERONET data provided interesting ancillary  
 126 measurements to support and better understand our analysis, WVC being the most crucial one. In  
 127 addition, the AERONET  $F$ s agree with pyranometer measurements with a correlation better than 99%  
 128 and the relative difference varies from 0.98 to 1.02 (Garcia et al., 2008). Moreover, we tested the  
 129 analysis in two sites, Alta-Floresta and Goddard Space Flight Center (GSFC), by using pyranometer  
 130 measured fluxes  $F$  and found no significant difference of the results in these two sites, if compared to  
 131 the corresponding analysis using the AERONET-modeled fluxes instead (see Supplement Appendix A).

132

### 133 3. Results

134 As further examples of determining ADRE using regression analysis, we show  $F^{aer}$  and AOD data from  
 135 four sites in Fig. 2. In addition, the linear (dashed line) and nonlinear decay (solid line) fits to the data  
 136 are shown. The bar on the vertical axis represents the average (with STD) value for  $F^0$ . GSFC (39° N,  
 137 77° W) (SZA = 70°) (Fig. 2a) and Rio-Branco (10° S, 68° W) (SZA = 70°) (Fig. 2b) represent cases in  
 138 which the data are of sufficient quality for estimating ADRE: AOD values reach close zero with only

139 minor changes in WVC, aerosol optical properties and surface reflectance for a given AOD, resulting in  
140 a narrow spread in the data. In these cases, since the nonlinear decay represents a more realistic decay  
141 of radiation intensity (based on squared values of residuals), the intersection of the nonlinear fit with  
142 the AOD=0 axis (y-axis) is within the STD of the baseline value. Dhadnah (26° N, 56° E) (SZA = 70°)  
143 (Fig. 2c) and GSFC at SZA = 22° (Fig. 2d) are examples of more challenging cases: in Fig. 2c only  
144 data points with AOD > 0.2 exist so that a more extensive extrapolation is needed, and in Fig. 2d there  
145 is significant scatter in the points.

146 Perhaps the most interesting feature shown in Fig. 2, which also significantly affects the quality  
147 of ADRE estimation, is the correlation of  $F^0$  with AOD. In Fig. 2a-d there is a negative correlation  
148 while in 2b the correlation is positive. The negative correlation between  $F^0$  and AOD is indirectly  
149 caused mainly by a positive correlation of AOD with WVC due to humid airmasses with large aerosol  
150 concentration. Only in some cases, where airmasses are dominated by dust aerosols, the correlation is  
151 negative. With increasing AOD and WVC, the WVC dims an increasing fraction of the radiation  
152 intensity – resulting in a smaller  $F^0$ . The opposite occurs if AOD and WVC have a negative correlation.  
153 Increase in the AOD as a function of WVC is presumably partly due to hygroscopic growth (e.g.,  
154 Kitamori et al., 2009), although probably a major part of the correlation can be attributed to a large  
155 variance in atmospheric conditions of aerosol properties and air humidity during seasons.

156 The intersections of the nonlinear decay fits (solid lines in Fig. 2) with the AOD = 0 axis –  
157 313.5 W/m<sup>2</sup> (Fig. 2a), 295.9 W/m<sup>2</sup> (2b), 327.4 W/m<sup>2</sup> (2c) and 1008.9 W/m<sup>2</sup> (2d) – approximate the  $F^0$   
158 value at AOD = 0. This is clear from the figure, if one imagines straight line fits through the circles and  
159 extrapolates fits down to AOD = 0. This approximation is, however, not necessarily a good one for the  
160 mean  $F^0$ , if  $F^0$  and AOD correlate (through the AOD-WVC-correlation). For the negative correlation  
161 cases (2a-d) the intersections of the nonlinear decay fits with the AOD = 0 axis tend to therefore over-  
162 estimate the mean baseline  $F^0$  (307.3 W/m<sup>2</sup> for 2a, 312.9 W/m<sup>2</sup> for 2c, and 972.1 W/m<sup>2</sup> for 2d) – as the

163 majority of  $F^0$  values are below the extrapolated  $F^0$ . Typically, for the positive correlation cases (2b,  
164 mean of  $F^0 = 303.4 \text{ W/m}^2$ ) the opposite occurs. As the linear fit obviously results in a lower estimation  
165 of  $F^0$ , the linear regression method can result often in a better estimation of the mean  $F^0$ , as is clearly  
166 the case in Fig. 2c (mean  $F^0 = 306.7 \text{ W/m}^2$ ) and Fig. 2d (mean  $F^0 = 973.0 \text{ W/m}^2$ ) – even if the nonlinear  
167 regression is physically more correct.

168         The performance of the two different regression methods and, in particular, the WVC and AOD  
169 correlation effect on the performance, is illustrated as scatter plots in Fig. 3. In Fig. 3a all data are  
170 presented in ADRE (nonlinear decay method) and ADRE (AERONET  $\Delta F^{average}$ , Eq. 2) form. The colour  
171 of the single points indicates the correlation of the WVC and AOD. In Fig. 3b the same is shown for the  
172 linear regression case. Evidently a majority of the cases are such that WVC and AOD have a strong  
173 positive correlation (red colored points). In addition, it seems that for most of these cases, the linear  
174 regression method (Fig. 3b) results in a better ADRE estimation than the nonlinear decay regression  
175 method (Fig. 3a). This means that the inaccuracy inherent in the linear regression cancels out errors  
176 caused by the WVC and AOD correlation. For a weak WVC and AOD correlation, the nonlinear decay  
177 method appears to be clearly better. Other parameters as surface albedo, ASYM or SSA do not play as a  
178 crucial role as WVC. We classified the ADRE estimates of the both methods against the baseline in  
179 respect of AOD, albedo, ASYM, SSA and WVC. It was evident that only WVC can explain the  
180 observed differences of both methods when compared against the baseline (see Supplement Appendix  
181 B). Moreover, we confirmed, by modeling a short wavelength range (310 nm -500 nm), that this WVC-  
182 effect vanishes, if some other wavelength band as e.g. the visible range of 400-700 nm containing no  
183 significant water vapour absorption is under consideration, instead of the broadband wavelength range  
184 of  $F^{aer}$  (see Supplement Appendix C).

185         Next we investigated possible geographical features of this correlation. Figure 4 shows the  
186 WVC and AOD correlation (in the color scales) at all the sites available from AERONET, in this case



187 for seasons; December-February (DJF, Fig. 4a), March-May (MAM, Fig. 4b), June-August (JJA, Fig.  
188 4c) and September-November (SON, Fig. 4d)(all years available). Most of the points are colored either  
189 green or red, indicating an absent or a positive correlation. The strongest positive correlation is for the  
190 stations in Europe and eastern USA, presumably due to aerosol hygroscopic growth. This holds  
191 especially for the JJA and SON- seasons The DJF and MAM- seasons provide weaker positive  
192 correlation, indicating that the linear method can then provide there somewhat underestimated ADRE.  
193 Interestingly, the strongest negative correlation appears during the JJA-season in the west Sahara's  
194 region and Central-America, probably caused by a strong desert dust domination and low WVC in the  
195 Saharan outflow region (Marsham et al., 2008). During those particular cases, the linear method can  
196 significantly underestimate ADRE, as indicated by the points of largest negative WVC vs. AOD  
197 correlation in Fig. 3b, while the nonlinear decay provides then a better estimate.

198 Finally, the ADRE estimations of all data are grouped together in numerical form in Table 1. As  
199 already evident from the figures, the nonlinear decay regression method overestimates (mean = -57.2  
200  $\text{Wm}^{-2}$ ) while the linear method underestimates (mean = -39.4  $\text{Wm}^{-2}$ ) the magnitude of ADRE  
201 (AERONET value = -46.1  $\text{Wm}^{-2}$ ). Overall, the linear method yields better results than the nonlinear  
202 decay method.

203 Previous studies have shown that the AERONET WVC agrees well with radiosonde sounding  
204 data (e.g., Prasad and Singh, 2009; Bokoye et al., 2007). Also, Smirnov et al. (2004) indicates that the  
205 AERONET WVC provides the root mean square difference of 7.0 % in a multiyear comparison with  
206 WVC measurements derived from GPS. We also compared AERONET WVC measurements against  
207 radiosonde data from five sites (Alta-Floresta, Cuiaba-Miranda, Niamey, Thessaloniki and Wallops)  
208 and observed similarly high correlations between these two data sources. However, we wanted to  
209 assess in particular whether there exists any systematic dependence between WVC from these two data  
210 sources as a function of AOD, which could affect our ADRE analysis based on the modeled  $F$ . We

211 found that while the ratio between the AERONET and radiosonde WVC is essentially constant for  
212 AODs (at 500nm) larger than about 0.1, in many sites WVC can deviate for the cases of smallest AOD  
213 (below 0.1). We estimated how our ADRE values (based on the  $F$  and AOD relation) would change if  
214 we normalized the AERONET-modeled fluxes to incorporate the WVC from the radiosonde  
215 measurements instead of AERONET-measured WVC. We found that the increased WVC uncertainty at  
216 the lowest AOD values introduces an insignificant change in our ADRE estimates.

217

#### 218 **4. Conclusions**

219 Determining the ADRE at the Earth's surface from radiative flux,  $F$ , measurements is not  
220 straightforward because it involves the estimation of the flux without aerosols  $F^0$ . This requires either  
221 radiative transfer modelling or an extrapolation of  $F$  down to AOD = 0.

222 We have evaluated two such extrapolation methods: i) a linear fit and ii) an nonlinear decay fit  
223 to the  $F$  and AOD data. As a reference we used the AERONET ADRE data in which  $F^0$  (and  $F$ ) is  
224 calculated with radiative transfer modelling. Radiation attenuation due to multiple scattering and  
225 absorption results typically in a near nonlinear decay of the intensity, and thus the nonlinear decay  
226 regression is expected to give a better estimation of ADRE. This would be the case if the typically  
227 positive correlation of WVC and AOD would not affect the dependency.  $F^0$  represents an  
228 unrealistically low WVC, resulting in an underestimation of attenuation caused by the WVC, and hence  
229 a too large  $F^0$ . This leads to an overestimation of the magnitude of ADRE. For stations and data series  
230 in which there is no correlation between WVC and AOD, the nonlinear decay fit is superior.

231 As the WVC effect was found to be of such importance, we also investigated the geographical  
232 correlation of WVC and AOD. The positive correlations clearly dominate, and clear negative  
233 correlations occur predominantly in desert dust dominated data series, such as the regions at the

234 Saharan outflow. The strongest positive correlation was found in in stations in Europe and Eastern  
235 USA. Our results indicate that the regression method, either linear or nonlinear, can readily produce a  
236 significant error due to the correlation of WVC and AOD. Since for a majority of locations, AOD and  
237 water vapour column (WVC) have a positive correlation, the linear method gives somewhat better  
238 results in general than the nonlinear approach, for the reasons discussed above. However, there are  
239 specific regions of strong negative WVC and AOD correlation, most notably in the Saharan dust  
240 outflow region, where the opposite takes place and nonlinear approach results in better estimate for  
241 ADRE. Therefore, based on our results we recommend that when the surface ADRE is estimated by  
242 using pyranometer and AOD measurements, the site-specific correlation between WVC and AOD  
243 should be also estimated to deduce whether linear or nonlinear approach is more suitable. We moreover  
244 recommend to take a one step forward and additionally attempt to correct for the possible bias due to  
245 WVC and AOD correlation. If the data for the WVC is available, then better ADRE accuracy is likely  
246 achieved if the flux measurements are normalized to constant WVC amount with simple scaling  
247 obtained from RT modeling.

248

#### 249 **Acknowledgments.**

250 We thank the AERONET team, principal investigators and other participants for theirs effort in  
251 establishing and maintaining the network. This study is supported by the Academy of Finland Doctoral  
252 Programme ACCC and the Maj and Tor Nessling foundation. We also thank Larry Oolman from  
253 Department of Atmospheric Science, University of Wyoming, for providing radiosonde- data of  
254 atmospheric water vapour column abundance.

255

#### 256 **References**

257 Bokoye, A. I., Royer, A., Cliche, P., and O'Neill, N.: Calibration of Sun Radiometer – based  
258 atmospheric water vapor retrievals using GPS meteorology, *J. Atmos. Ocean. Tech.*, 24,  
259 964–979, doi:10.1175/JTECH2011.1, 2007.

260 Bush, B. C. and Valero, F. P. J.: Spectral aerosol radiative forcing at the surface during the Indian  
261 Ocean Experiment (INDOEX), *J. Geophys. Res.*, 107, 8003, doi:10.1029/2000JD000020,  
262 2002.

263 Bush, B. C. and Valero, F. P. J.: Surface aerosol radiative forcing at Gosan during the ACE-Asia  
264 campaign, *J. Geophys. Res.*, 108, 8660, doi:10.1029/2002JD003233, 2003.

265 Conant, W. C., Seinfeld, J. H., Wang, J., Carmichael, G. R., Tang, Y., Uno, I., Flatau, P. J.,  
266 Markowicz, K. M., and Quinn, P. K.: A model for the radiative forcing during ACE-Asia derived  
267 from CIRPAS Twin Otter and R/V Ronald H. Brown data and comparison with observations, *J.*  
268 *Geophys. Res.*, 108, 8661, doi:10.1029/2002JD003260, 2003.

269 Derimian, Y., Léon, J.-F., Dubovik, O., Chiapello, I., Tanré, D., Sinyuk, A., Auriol, F., Podvin, T.,  
270 Brogniez, G., and Holben, B. N.: Radiative properties of aerosol mixture observed during the  
271 dry season 2006 over M'Bour, Senegal (African Monsoon Multidisciplinary Analysis campaign),  
272 *J. Geophys. Res.*, 113, D00C09, doi:10.1029/2008JD009904, 2008.

273 Di Sarra, A., Pace, G., Meloni, D., De Silvestri, L., Piacentino, S., and Monteleone, F.: Surface  
274 shortwave radiative forcing of different aerosol types in the central Mediterranean, *Geophys.*  
275 *Res. Lett.*, 35, L02714, doi:10.1029/2007GL032395, 2008.

276 Dubovik, O., and M. D. King, A flexible inversion algorithm for retrieval of aerosol optical properties  
277 from Sun and sky radiance measurements, *J. Geophys. Res.*, 105(D16), 20673–20696,  
278 doi:[10.1029/2000JD900282](https://doi.org/10.1029/2000JD900282), 2000.

279 Dubovik, O., Smirnov, A., Holben, B. N., King, M. D., Kaufman, Y. J., Eck, T. F., and Slutsker, I.:  
280 Accuracy assessments of aerosol optical properties retrieved from Aerosol Robotic Network  
281 (AERONET) Sun and sky radiance measurements, *J. Geophys. Res.*, 105, 9791–9806,  
282 doi:10.1029/2000JD900040, 2000.

283 Dumka, U. C., Satheesh, S. K., Pant, P., Hegde, P., and Krishna Moorthy, K.: Surface changes  
284 in solar irradiance due to aerosols over central Himalayas, *Geophys. Res. Lett.*, 33, L20809,  
285 doi:10.1029/2006GL027814, 2006.

286 Eck, T. F., B. N. Holben, J. S. Reid, O. Dubovik, A. Smirnov, N. T. O'Neill, I. Slutsker, and S. Kinne,  
287 Wavelength dependence of the optical depth of biomass burning, urban, and desert dust aerosols, *J.*  
288 *Geophys. Res.*, 104(D24), 31333–31349, doi:10.1029/1999JD900923, 1999.

289 García O. E., Díaz, A. M., Expósito, F. J., Díaz, J. P., Dubovik, O., Dubuisson, P., Roger, J.-  
290 C., Eck, T. F., Sinyuk, A., Derimian, Y., Dutton, E. G., Schafer, J. S., Holben, B. N., and  
291 García, C. A.: Validation of AERONET estimates of atmospheric solar surface fluxes and

292 aerosol radiative forcing by ground-based broadband measurements, *J. Geophys. Res.*, 113,  
293 D21207, doi:10.1029/2008JD010211, 2008.

294 García O. E., Díaz, A. M., Expósito, F. J., Díaz, J. P., Redondas, A., and Sasaki, T.: Aerosol  
295 radiative forcing and forcing efficiency in the UVB for regions affected by Saharan and Asian  
296 Mineral Dust, *J. Atmos. Sci.*, 66, 1033–1040, doi:10.1175/2008JAS2816.1, 2009.

297 García O.E., Díaz J.P., Expósito F.J., Díaz A.M., Dubovik O. and Derimian Y. Aerosol Radiative  
298 Forcing: AERONET-Based Estimates, *Climate Models*, Dr. Leonard Druyan (Ed.), ISBN: 978-953-51-  
299 0135-2, InTech, DOI: 10.5772/32287. Available from: [http://www.intechopen.com/books/climate-  
300 models/aerosol-radiative-forcing-aeronet-based-estimates](http://www.intechopen.com/books/climate-models/aerosol-radiative-forcing-aeronet-based-estimates), 275-296, 2012.

301 Holben, B. N., Eck, T. F., Slutsker, I., Tanré, D., Buis, J. P., Setzer, A., Vermote, E., Reagan, J. A.,  
302 Kaufman, Y. J., Nakajima, T., Lavenu, F., Jankowiak, I., and Smirnov, A.: AERONET – a Federated  
303 Instrument Network and Data Archive for aerosol characterization, *Remote Sens. Environ.*, 66, 1–16, doi:10.1016/S0034-4257(98)00031-5, 1998.

304 Intergovernmental Panel on Climate Change (IPCC): *Climate Change 2013: The Physical Science  
305 Basis*, available at: <http://www.ipcc.ch/> (last access: January 2014), 2013.

306 Kaufman, Y. J., Tanré, D., Holben, B. N., Mattoo, S., Remer, L. A., Eck, T. F., Vaughan, J.,  
307 Chatenet, B.: Aerosol radiative impact on spectral solar flux at the surface, derived  
308 from principal-plane sky measurements, *J. Atmos. Sci.*, 59, 635–646, doi:10.1175/1520-  
309 0469(2002)059<0635:AROSS>2.0.CO;2, 2002.

310 Kitamori, Y., Mochida, M., and Kawamura, K.: Assessment of the aerosol water content in urban  
311 atmospheric particles by the hygroscopic growth measurements in Sapporo, Japan, *Atmos.  
312 Environ.*, 43, 3416–3423, 2009.

313 Kudo, R., Uchiyama, A., Yamazaki, A., Sakami, T., and Kobayashi, E.: From solar radiation  
314 measurements to optical properties: 1998–2008 trends in Japan, *Geophys. Res. Lett.*, 37,  
315 L04805, doi:10.1029/2009GL041794, 2010.

316 Loeb, N. G. and Su, W.: Direct aerosol radiative forcing uncertainty based on a radiative perturbation  
317 analysis, *J. Climate*, 23, 5288–5293, doi:10.1175/2010JCLI3543.1, 2010.

318 Markowicz, K. M., Flatau, P. J., Remiszewska, J., Witek, M., Reid, E. A., Reid, J. S., Bucholtz, A.,  
319 and Holden, B.: Observations and modeling of the surface aerosol radiative forcing during  
320 UAE2, *J. Atmos. Sci.*, 65, 2877–2891, doi:10.1175/2007JAS2555.1, 2008.

321 Marsham, J. H., Parker, D. J., Grams, C. M., Johnson, B. T., Grey, W. M. F., and Ross, A. N.:  
322 Observations of mesoscale and boundary-layer scale circulations affecting dust transport  
323 and uplift over the Sahara, *Atmos. Chem. Phys.*, 8, 6979–6993, doi:10.5194/acp-8-6979-  
324 2008, 2008.

325

326 Myhre, G.: Consistency between satellite-derived and modeled estimates of the direct aerosol  
 327 effect, *Science*, 325, 187, doi:10.1126/science.1174461, 2009.

328 Prasad, A. K. and Singh, R. P.: Validation of MODIS Terra, AIRS, NCEP/DOE AMIP-II  
 329 Reanalysis-2, and AERONET Sun photometer derived integrated precipitable water vapor  
 330 using ground-based GPS receivers over India, *J. Geophys. Res.*, 114, D05107,  
 331 doi:10.1029/2008JD011230, 2009.

332 Roger, J. C., Mallet, M., Dubuisson, P., Cachier, H., Vermote, E., Dubovik, O., and De  
 333 spiau, S.: A synergetic approach for estimating the local direct aerosol forcing: application  
 334 to an urban zone during the Expérience sur Site pour Contraindre les Modèles de Pollution  
 335 et de Transport d'Emission (ESCOMPTE) experiment, *J. Geophys. Res.*, 111, D13208,  
 336 doi:10.1029/2005JD006361, 2006.

337 Satheesh, S. K. and Ramanathan, V.: Large differences in tropical aerosol forcing at the top of  
 338 the atmosphere and Earth's surface, *Nature*, 405, 60–63, doi:10.1038/35011039, 2000.

339 Satheesh, S. K., Vinoj, V., and Krishna Moorthy, K.: Radiative effects of aerosols at an urban  
 340 location in southern India: Observations vs. model, *Atmos. Environ.*, 44, 5295–5304,  
 341 doi:10.1016/j.atmosenv.2010.07.020, 2010.

342 Smirnov, A., B. N. Holben, A. Lyapustin, I. Slutsker, and T. F. Eck, AERONET processing algorithm  
 343 refinement, paper presented at AERONET Workshop, Univ. of Huelva and the Span. Soc. of Optics, El  
 344 Arenosillo, Spain, May 10-14, 2004.

345 Table 1. The estimated ADRE( $F^{aer}$ ) with standard deviations compared with the AERONET value.

346 MAD = Mean Absolute Deviation. Units are in  $Wm^{-2}$ , except for the correlation coefficient (CC).

Parameter	AERONET	Method	Estimate	Est. - AERONET	CC	MAD
ADRE	$-46.1 \pm 20.4$	Exp. decay	$-57.2 \pm 23.4$	-11.1	0.75	13.4
		Linear	$-39.4 \pm 16.9$	+6.7	0.89	8.9

347

348

349

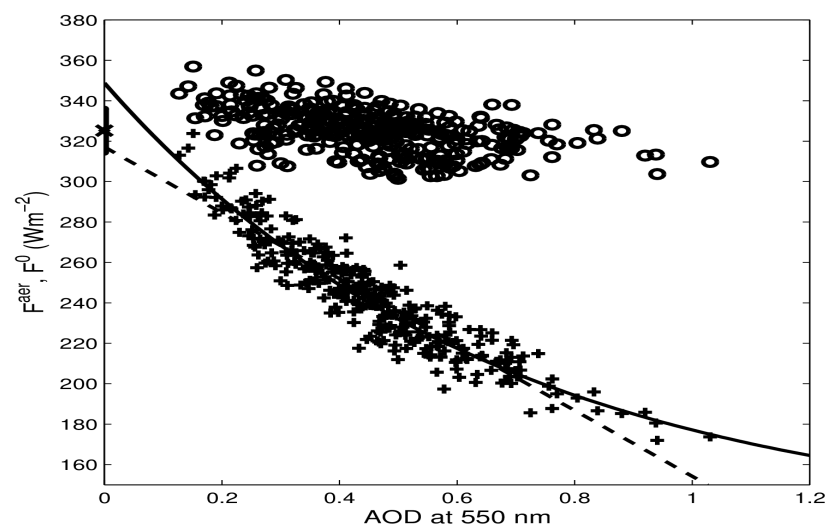
350

351

352

353

14



354

355

356

357

358

359

360

361

362 Figure 1: Radiative flux with aerosols  $F^{aer}$  (plusses) and without aerosols  $F^0$  (circles) as a function of  
363 AOD for the AERONETsite in Kanpur in March-May and with  $SZA = 69^\circ \pm 1.5^\circ$ . The bar on the  
364 vertical axis represents the mean value of the estimated  $F^0$  (all circles). The solid and dashed lines  
365 represent the exponential and linear fits to the data, respectively.

366

367

368

369

370

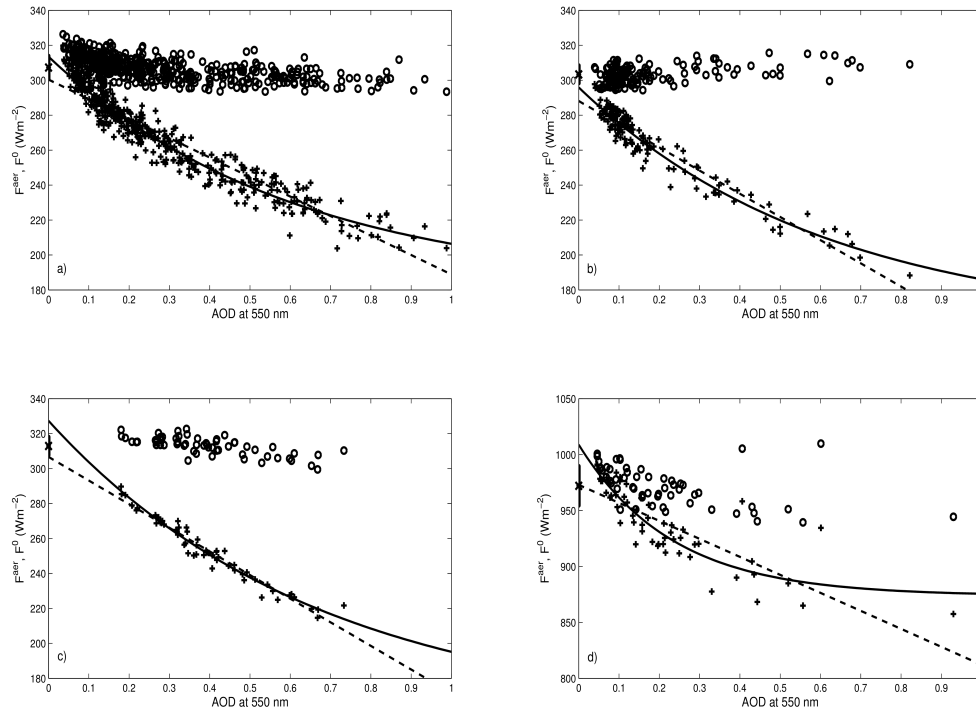
371

372

373

374

375



376 Figure 2: Same as Fig. 1, but for the June-August season in a) GSFC (SZA=70°), b) Rio-Branco (SZA  
 377 = 70°), c) Dhadnah (SZA = 70°), d) GSFC (SZA = 22°).

378  
 379  
 380  
 381  
 382  
 383  
 384  
 385  
 386  
 387  
 388  
 389  
 390  
 391  
 392  
 393  
 394  
 395  
 396



397  
398  
399  
400  
401  
402  
403  
404  
405  
406  
407  
408  
409  
410  
411  
412  
413  
414  
415  
416  
417  
418  
419  
420  
421  
422  
423  
424  
425  
426  
427  
428  
429

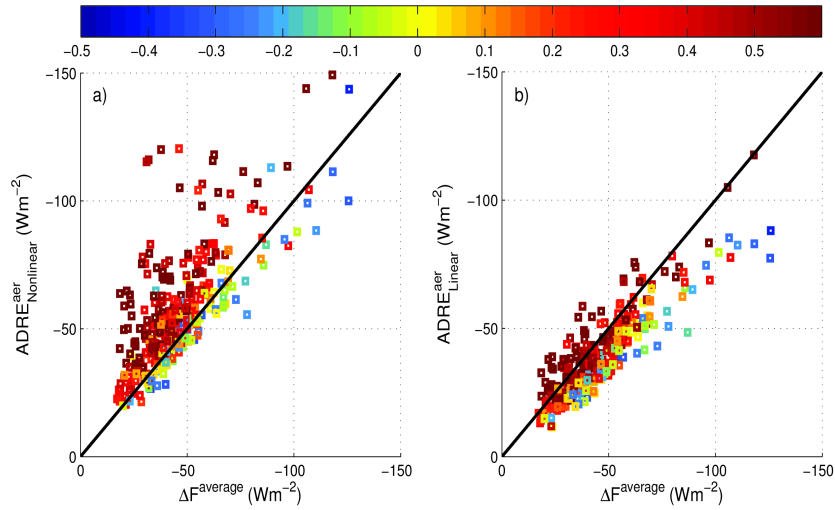
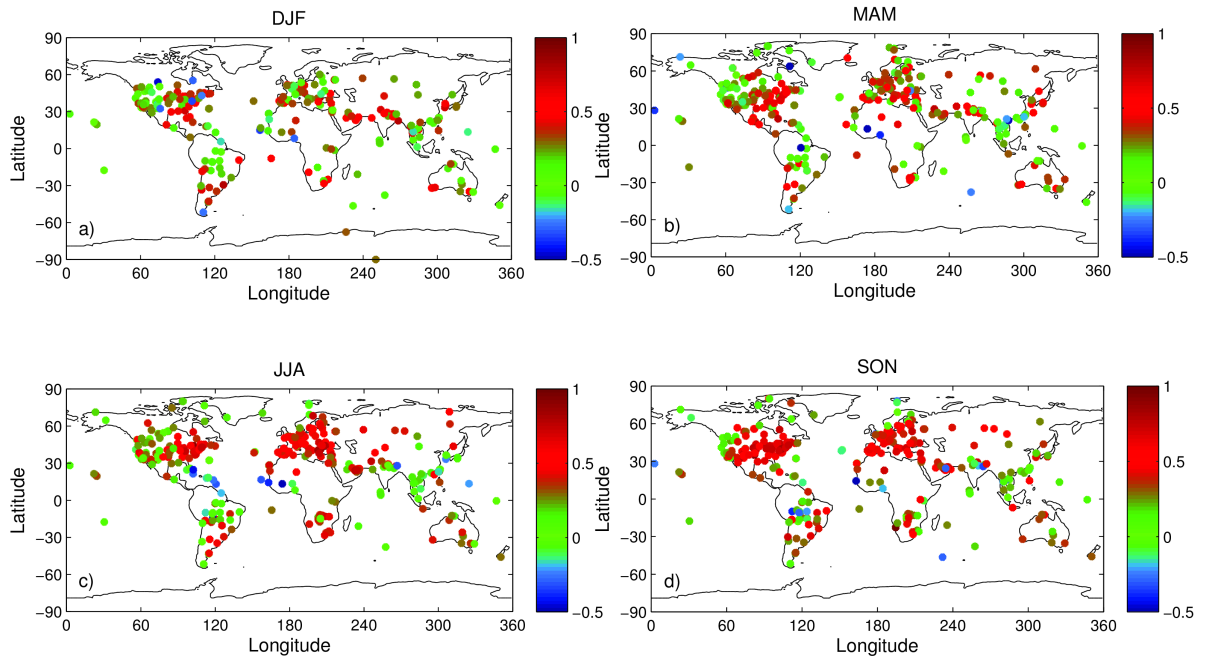


Figure 3: ADRE predicted with exponential decay (a) and linear (b) regression methods (equation 1), compared with AERONET values (equation 2). The color of the data points represents the correlation coefficient of the AOD and WVC correlation, with red color indicating positive and blue color negative correlation.



431  
 432  
 433  
 434  
 435  
 436  
 437  
 438  
 439

440 Figure 4: Geographical distribution of the AOD and WVC correlation, at all AERONET stations  
 441 considered in this study for a) December-February, b) March-May, c) June-August and d) September-  
 442 November (all available years).